R990

ORNL/TM-7517

ornl

OAK
RIDGE
NATIONAL
LABORATORY

UNION
CARBIDE

Dependence of Stability of Metastable Superconductors on Copper Fraction

S. A. Elrod
J. W. Lue
J. R. Miller
L. Dresner

OPERATED BY
UNION CARBIDE CORPORATION
FOR THE UNITED STATES
DEPARTMENT OF ENERGY

CONTENTS

ABSTRACT

The stability of composite superconductors operating in the metastable regime depends upon such factors as matrix resistivity, cooled surface dimensions, fraction of critical current, and volume fraction of stabilizer. By assuming constant thermophysical properties, we developed analytic expressions for the energy and voltage of the minimum propagating zone (MPZ). With other factors held constant, these expressions have been used to predict composite superconductor stability as a function of copper fraction: lower copper fractions lead to higher MPZ energies. MPZ voltages have been measured for three NbTi/Cu composites having different copper fractions and different critical current densities for several magnetic fields and transport currents. Experimental MPZ voltages have been used to calculate an effective heat transfer coefficient, which is subsequently used to calculate the MPZ energy. The experimental MPZ energies support the theoretical expectation that lower copper fractions lead to higher stability in the metastable regime.

1. INTRODUCTION

If subjected to a large enough perturbation, a metastable superconducting magnet will quench. As a result, the magnet designer often tries to choose the conductor that can sustain the largest perturbation without quenching. In Sect. 5 it is shown that for metastable conductors low copper fractions are to be preferred. To test this conclusion, we have studied the dependence of the minimum propagating zone (MPZ) energy (E) on copper-to-superconductor ratio for NbTi/Cu superconductors having nearly identical geometries ($A = 6.1 \times 10^{-6}$ m^2, $P = 2.7 \times 10^{-3}$ m) but having copper fractions (f) of 0.85, 0.84, and 0.79 and NbTi critical current densities (J_{csc}) of 4.7×10^8, 4.5×10^8, and 7.7×10^8 Am^{-2}, respectively, at 4.2 K and 7.5 T. [We assume in this paper that the minimum quench energy (MQE) and E provide consistent measures of conductor stability.]

In this experiment electrical heaters bonded to the conductor surface are pulsed to provide the initial perturbation. Losses to the adjacent epoxy potting are not negligible and cannot be assumed constant for the three conductors. It is, therefore, not possible to measure the MQE reliably. More importantly, K. Ishibashi et al.[1] show that the critical temperature profile generated by applying the MQE to a given conductor is not necessarily the steady-state profile given by the MPZ theory.[2] Rather, the critical profile and the value of the MQE depend upon the spatial and temporal distribution of the initial disturbance. But, Ishibashi et al. do report that for perturbations of small extent ($\Delta x \leq 2$ cm) and short duration ($\Delta t \leq 2$ ms), the critical profile closely approximates the MPZ profile and remains stable for a significant period of time. It is only for larger Δx or Δt that the critical profile differs significantly from the MPZ profile. This suggests the following experimental procedure:

(1) Apply heat pulses having identical, small Δx and Δt ($\Delta t = 1$ ms, $\Delta x = 1$ cm). Vary only the intensity of the heat pulse.

(2) Experimentally determine which heat pulse generates a nearly steady critical profile.

(3) Use the measured voltage drop across this critical profile to determine E.

2. BASIC EQUATIONS

If we assume constant thermophysical properties, we can derive simple, closed formulas of considerable heuristic value for the voltage, energy, and central temperature of MPZs. We begin with a steady-state heat balance for a unit length of composite superconductor:

$$\frac{d}{dx}\left(k\frac{dT}{dx}\right) + Q_J - \frac{hP}{A}(T - T_b) = 0 \ . \tag{1}$$

(All symbols are defined in a list at the end of the paper.) We reduce the order of this differential equation by using the substitution of Maddock, James, and Norris,[3] $s = k(dT/dx)$:

$$s\frac{ds}{dT} + k\left[Q_J - \frac{hP}{A}(T - T_b)\right] = 0 \ . \tag{2}$$

If we introduce dimensionless variables, Eq. (2) becomes

$$y\frac{dy}{d\tau} + \alpha i^2 g(\tau) - \tau = 0 \ , \tag{3}$$

where $g(\tau)$ is the function of Keilin et al.[4] and Maddock et al.:[3]

$$g(\tau) = \begin{cases} 0 & 1 - i \geqslant \tau \\ (\tau + i - 1)/i & 1 - i < \tau < 1 \\ 1 & \tau \geqslant 1 \end{cases} \ . \tag{4}$$

The function $g(\tau)$ gives the fraction of the current flowing in the copper as a function of temperature. Use of this function is equivalent to assuming a linear relation between temperature and critical current. In the range of temperatures $\tau < 1 - i$, the conductor is superconducting; in the range $1 - i < \tau < 1$, it is current-sharing; and, for $\tau > 1$, it is normal.

3. CONNECTION BETWEEN MPZ VOLTAGE AND ENERGY

The MPZ energy is given by

$$E = \int_{-\infty}^{\infty} S(T - T_b)A \, dx = 2 \int_{T_b}^{T_{max}} \frac{kS(T - T_b)A}{s} \, dT \tag{5a}$$

$$= 2 \left(\frac{kA}{hP}\right)^{1/2} S(T_{cr} - T_b)A \int_0^{\tau_0} \frac{\tau \, d\tau}{y} . \tag{5b}$$

The voltage dV across an element dx of the normal zone is equal to the resistance of the copper path $\rho dx/fA$ times the current $Ig(\tau)$ flowing in the copper. Thus,

$$V = \int_{-\infty}^{\infty} \frac{\rho I g(\tau)}{fA} \, dx = 2 \int_0^{T_{max}} \frac{I\rho k}{sfA} \, g(\tau) \, dT \tag{6a}$$

$$= 2\left(\frac{kA}{hP}\right)^{1/2} \frac{I\rho}{fA} \int_0^{\tau_0} \frac{g(\tau)}{y} \, d\tau . \tag{6b}$$

If we divide Eq. (3) by y and integrate between $\tau = 0$ and $\tau = \tau_0$, we find

$$\alpha i^2 \int_0^{\tau_0} \frac{g(\tau)}{y} \, d\tau = \int_0^{\tau_0} \frac{\tau}{y} \, d\tau , \tag{7}$$

since $y = 0$ at both $\tau = 0$ and $\tau = \tau_0$. From (7), (6b), and (5b), it follows that

$$E = \frac{VIAS}{Ph} . \tag{8}$$

This relation connects the MPZ energy (E) with the MPZ voltage (V), a conveniently measured quantity. It is interesting that relation (8) has been obtained without solving the differential Eq. (3) and that it applies independently of the precise form of the function $g(\tau)$. It does, however, depend on the assumption of constant thermophysical properties.

4. CALCULATION OF THE MPZ

If we integrate Eq. (3) as it stands from 0 to τ_0, we find

$$\int_0^{\tau_0} [\alpha i^2 g(\tau) - \tau] \, d\tau = 0 \ ,$$

which requires the equality of the two shaded areas shown in Fig. 1.

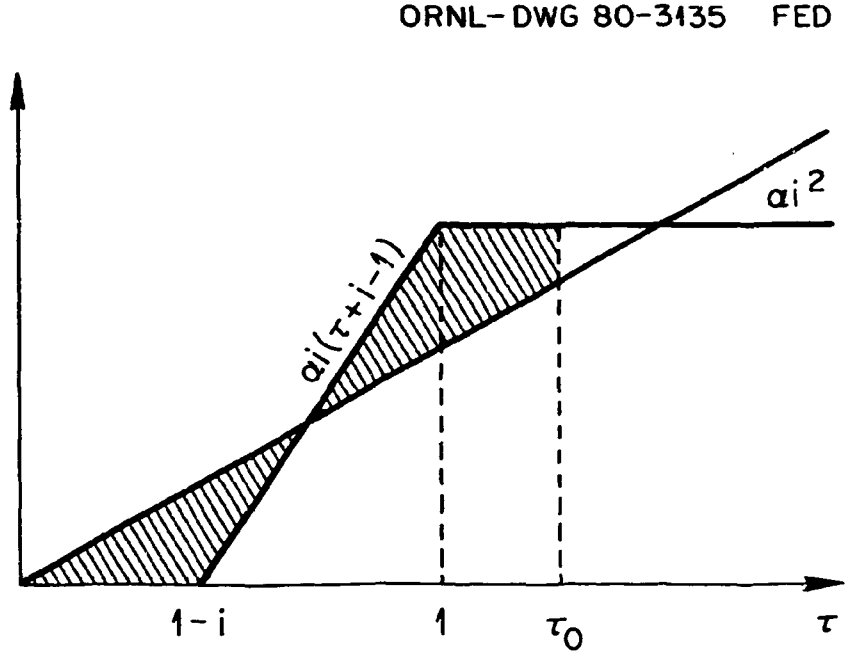

Fig. 1. A sketch illustrating the determination of the maximum temperature of the minimum propagating zone with the equal-area criterion.

If $\tau_0 < 1$ (small MPZs, low stability), then it can be shown easily from Fig. 1 that

$$\tau_0 = (1 - i) \frac{\sqrt{\alpha i}}{\sqrt{\alpha i} - 1} \ . \qquad (9)$$

In terms of α and i, the condition $\tau_0 < 1$ for (9) becomes $\alpha i^3 > 1$. When $\tau_0 < 1$, Eq. (3) can be solved to give

$$y = \tau \qquad 0 < \tau < 1 - i \,, \tag{10a}$$

$$y = [\tau^2 - \alpha i(\tau + i - 1)^2]^{1/2} \qquad 1 - i < \tau < \tau_0 \,. \tag{10b}$$

Thus,

$$\varepsilon = \int_0^{\tau_0} \frac{\tau}{y}\, d\tau = (1 - i) + \int_{1-i}^{\tau_0} \frac{\tau\, d\tau}{[\tau^2 - \alpha i(\tau + i - 1)^2]^{1/2}} \,, \tag{11a}$$

or, after some tedious computation,

$$\frac{\varepsilon}{1 - i} = \frac{\alpha i}{\alpha i - 1}\left[1 + \frac{\frac{\pi}{2} + \arcsin\left(\frac{1}{\sqrt{\alpha i}}\right)}{\sqrt{\alpha i - 1}}\right] . \tag{11b}$$

Using Eq. (11b), we can calculate contours of constant dimensionless MPZ energy (ε) in the α-i plane. First, we plot the right-hand side of Eq. (11b) as a function of αi. Then, we fix ε and choose a value of i. We can determine αi and, thus, α from the value of $\varepsilon/(1 - i)$, which we can now calculate, and from the plot made in the first step. Figure 2 shows such contours for $\varepsilon = 0.25$, 0.50, and 1.0. Figure 2 also shows the locus $C_1{:}\alpha i^2 = 2 - i$ that separates the cryostable from the metastable part of the α-i plane and the locus $C_2{:}\alpha i^3 = 1$. (The locus $C_0{:}\alpha i^2 = 1$ separates full recovery from cold-end recovery.) The contours for $\varepsilon = 0.25$, 0.50, and 1.0 all lie to the right of C_2 so that the condition $\alpha i^3 > 1$ is fulfilled along them, as it should be.

The locus C_1 corresponds to $\varepsilon = \infty$. When ε is large, we expect αi^3 to be <1 and τ_0 to be >1. In fact, for very large ε, τ_0 will be close to the equal-area value it would have on C_1, namely, $\tau_0 = \alpha i^2 = 2 - i > 1$. In such a case, we can avoid the labor involved in calculating ε exactly by replacing the three-part heat generation curve given in Eq. (4) by a two-part heat generation curve,

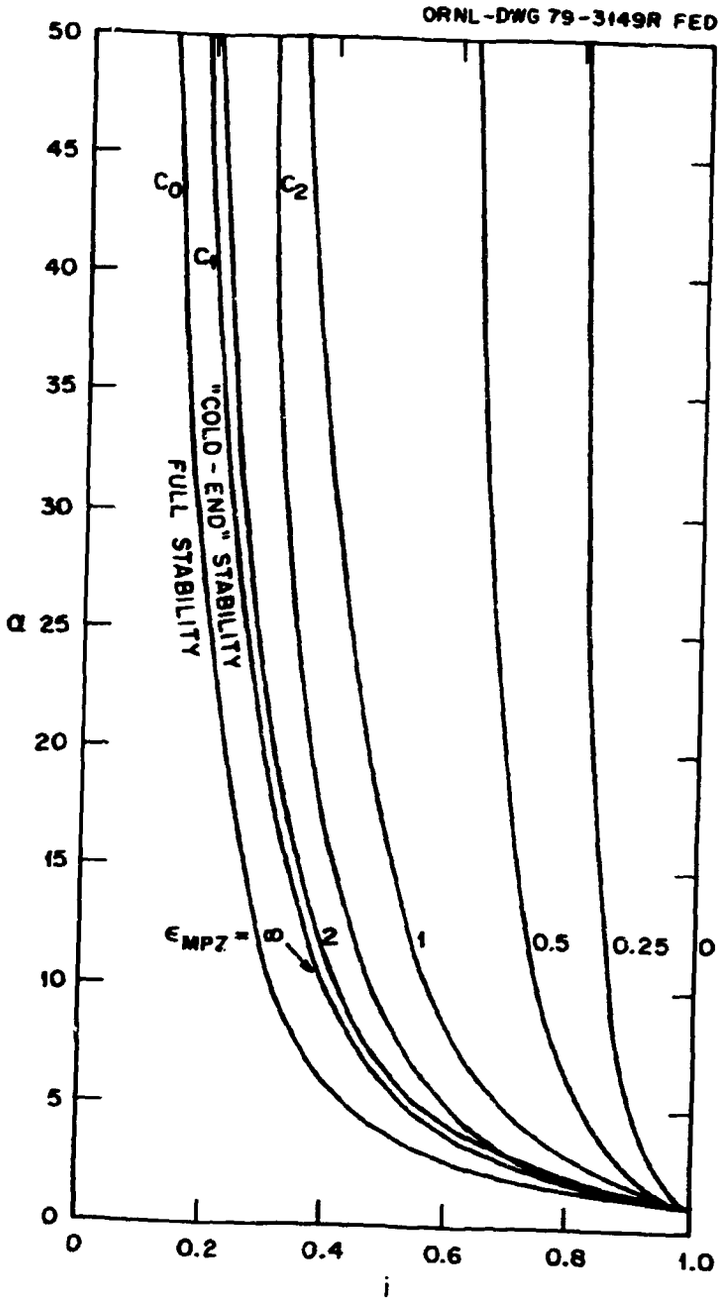

Fig. 2. Contours of the dimensionless MPZ energy ϵ in the α-i plane. The locus C_1 separates the cryostable from the metastable parts of the plane and the locus C_0 separates full recovery from cold-end recovery. The locus C_2 defines the region of validity of the approximate formula (14) for ϵ and is discussed in Sect. 4.

$$g(\tau) = \begin{cases} 0 & \tau < 1 - \frac{i}{2} \\ 1 & \tau > 1 - \frac{i}{2} \end{cases}, \tag{12}$$

in which a sudden transition occurs at the equal-area temperature[5] $\tau = 1 - i/2$. Then,

$$y = \tau \qquad 0 < \tau < 1 - \frac{i}{2}, \tag{13a}$$

$$y = \left[\tau^2 - 2\alpha i^2 \left(\tau + \frac{i}{2} - 1\right)\right]^{1/2} \qquad 1 - \frac{i}{2} < \tau, \tag{13b}$$

and

$$\tau_0 = \alpha i^2 \left(1 - \sqrt{1 - \frac{2 - i}{\alpha i^2}}\right). \tag{13c}$$

Integrating, we find

$$\epsilon = \int_0^{\tau_0} \frac{\tau}{y}\, d\tau = 1 - \frac{i}{2} + \int_{1-\frac{i}{2}}^{\tau_0} \frac{\tau\, d\tau}{[\tau^2 - 2\alpha i^2(\tau + \frac{i}{2} - 1)]^{1/2}} \tag{14a}$$

$$= \alpha i^2 \ln \left(1 - \frac{2 - i}{\alpha i^2}\right)^{-1/2}. \tag{14b}$$

Table 1 shows a comparison of Eqs. (11b) and (14b) along the boundary curve $C_2: \alpha i^3 = 1$. Agreement is quite good except for i near 1, where the curves C_2 and C_1 are very close together. Thus, we expect Eq. (14b) to be sufficiently reliable to sketch the general trend of higher ϵ contours in the α–i plane. Figure 2 shows the contour for $\epsilon = 2$ calculated using Eq. (14b).

Table 1. Comparison of Eqs. (11b) and (14b) along $\alpha i^3 = 1$

	ϵ	
i	Eq. (11b)	Eq. (14b)
0.2	1.13	1.12
0.3	1.22	1.19
0.4	1.33	1.28
0.5	1.47	1.39
0.6	1.66	1.53
0.7	1.94	1.72
0.8	2.41	2.01
0.9	3.45	2.56

5. USE OF THE ε CONTOURS TO SELECT A Cu/SC RATIO[6]

We can use the ε contours in Fig. 2 to determine the Cu/SC ratio of metastable conductors. Consider, for example, a candidate conductor intended for service at 8 T, 4.2 K, and an overall current density of 9×10^7 Am^{-2}. The conductor is to be a composite of NbTi, whose critical current density is 5.6×10^8 Am^{-2} at 8 T and 4.2 K, and copper, whose residual resistivity ratio is 160. With these data fixed,

$$\alpha = \frac{1.2 \times 10^8}{(Ph/A)} \frac{(1 - f)^2}{f} \quad (Ph/A \text{ in } Wm^{-3}K^{-1}) \tag{15a}$$

and

$$i = \frac{0.16}{1 - f} , \tag{15b}$$

where f is the volume fraction of copper in the composite. The quantity Ph/A is not usually very well known in the early stages of design, but for the conductor described above, a reasonable range of values is 2×10^5 to 5×10^6 $Wm^{-3}K^{-1}$. Figure 3 shows the loci traced out by Eqs. (15a,b) in the α-i plane as f varies for various values of Ph/A. If we fix the value of Ph/A (take Ph/A = 1×10^6 $Wm^{-3}K^{-1}$, for example) and superimpose the f locus on Fig. 2, the intersections of the f locus with the contours of constant ε give ε as a function of f. When f = 0.84 (Cu/SC = 5.25), the operating current equals the critical current, and ε = 0. Near the right-hand side of the graph, the f locus cuts the contours of constant ε steeply so that we start out moving rapidly from ε contour to ε contour as f decreases. However, as f continues to decrease, the f locus becomes nearly parallel to the contours of constant ε, and a point is reached at which further reduction of f brings little increase in stability. In the present example, the point of diminishing returns occurs at $i \sim 0.6$, for which f = 0.73 (Cu/SC = 2.70). When Cu/SC = 5 (f = 0.83, i = 0.96), ε is only one-sixth as large as it is for Cu/SC = 2.7, so the lower ratio is preferable.

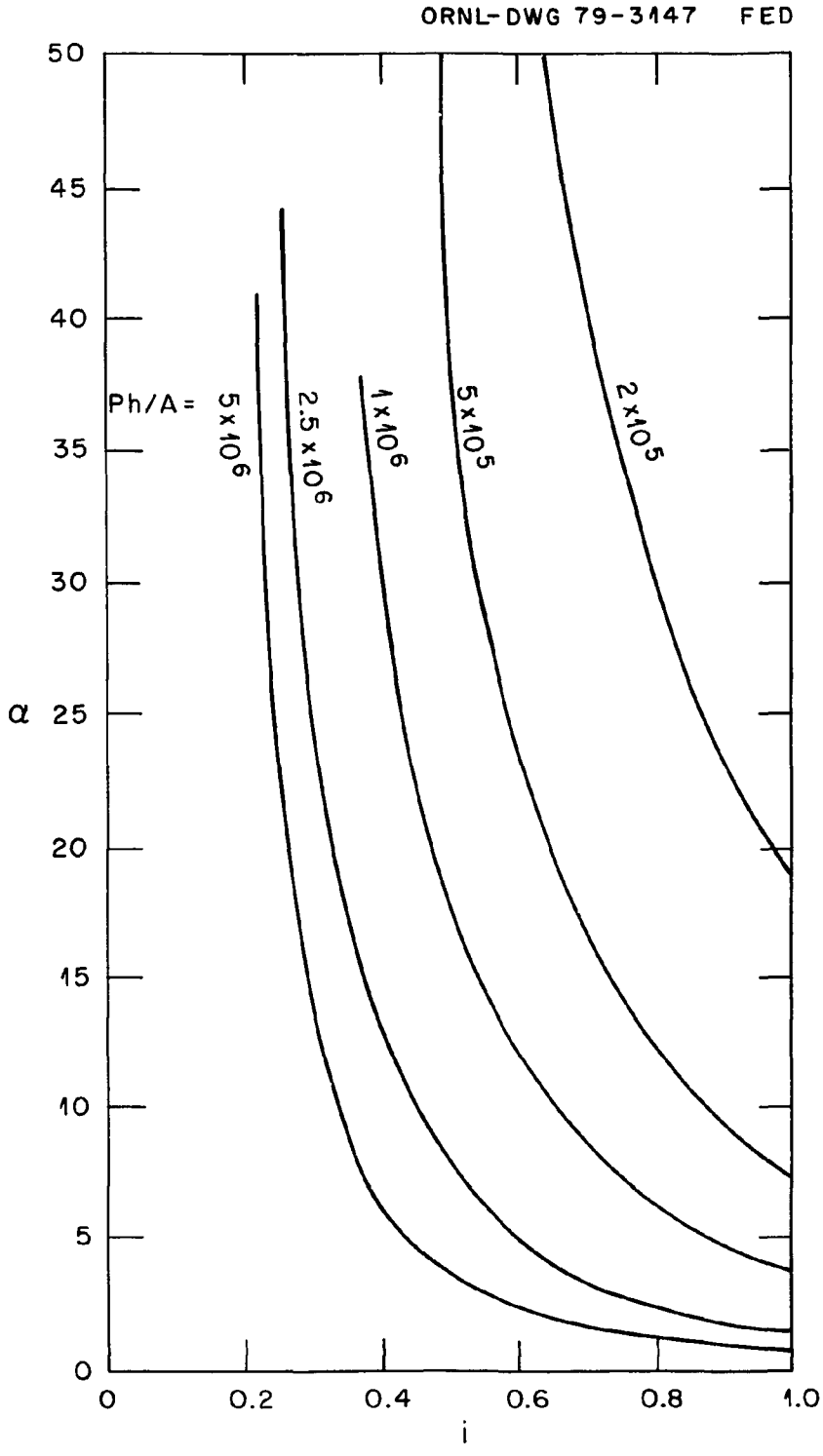

Fig. 3. The loci traced out by Eqs. (15) in the α-i plane as the copper fraction f varies, for several values of Ph/A.

We get the same conclusion no matter which f locus we consider up to values of Ph/A = 5×10^6 $Wm^{-3}K^{-1}$. For this value of Ph/A, it is possible to achieve cryostability (both cold-end and full stability). Paradoxically, to achieve cryostability when Ph/A is large, we need large Cu/SC ratios. However, for metastable conductors with smaller Ph/A, we prefer low Cu/SC ratios.

6. SAMPLE PREPARATION

To obtain test conductors having nearly identical geometries and different values of f, three NbTi/Cu composite conductors were soldered into U-shaped copper channels formed from a 5.6-mm × 0.56-mm copper strip. Data for the test conductors are provided in Table 2. A photograph of one of the finished conductor cross sections is shown in Fig. 4. The conductor was wound under tension in a helical groove machined in a G-10 fiberglass cylinder and potted in place with Emerson and Cummings 2850FT Stycast epoxy with one face exposed to the helium bath (see Fig. 5). The external magnetic field was applied parallel to the axis of the fiberglass cylinder.

Strain gauges (R = 120 Ω) bonded to the side of the conductor in contact with the fiberglass cylinder were used as heaters (see Fig. 5). A 1-cm heater was positioned at the center of each 3-m test conductor.

Seven voltage taps were soldered to the conductor at various locations. The voltage tap leads were co-wound with the conductor in the helical groove of the sample holder in order to reduce inductive pickup.

A schematic representation of the instrumentation is shown in Fig. 6.

Table 2. Conductor specifications

	Initial conductor			Test conductor		$\rho(\Omega m)$ and $J_{csc}(Am^{-2})$		
Sample	Dimensions (mm × mm)	Cu/SC	# Filaments	Total area (m^2)	Cu/SC	B = 6.0 T	7.0 T	7.5 T
1	2.54 × 1.27	2.55	18	6.2×10^{-6}	5.85	$J_{csc} = 7.8 \times 10^{8}$	$J_{csc} = 5.0 \times 10^{8}$	$J_{csc} = 4.7 \times 10^{8}$
						$\rho = 3.8 \times 10^{-10}$	$\rho = 4.1 \times 10^{-10}$	$\rho = 4.4 \times 10^{-10}$
2	2.54 × 1.27	2.19	18	6.2×10^{-6}	5.15	$J_{csc} = 7.4 \times 10^{8}$	$J_{csc} = 5.3 \times 10^{8}$	$J_{csc} = 4.5 \times 10^{8}$
						$\rho = 3.8 \times 10^{-10}$	$\rho = 4.2 \times 10^{-10}$	$\rho = 4.4 \times 10^{-10}$
3	2.49 × 1.24	1.36	1530	6.1×10^{-6}	3.65	$J_{csc} = 1.2 \times 10^{9}$	$J_{csc} = 9.1 \times 10^{8}$	$J_{csc} = 7.7 \times 10^{8}$
						$\rho = 3.9 \times 10^{-10}$	$\rho = 4.5 \times 10^{-10}$	$\rho = 4.7 \times 10^{-10}$

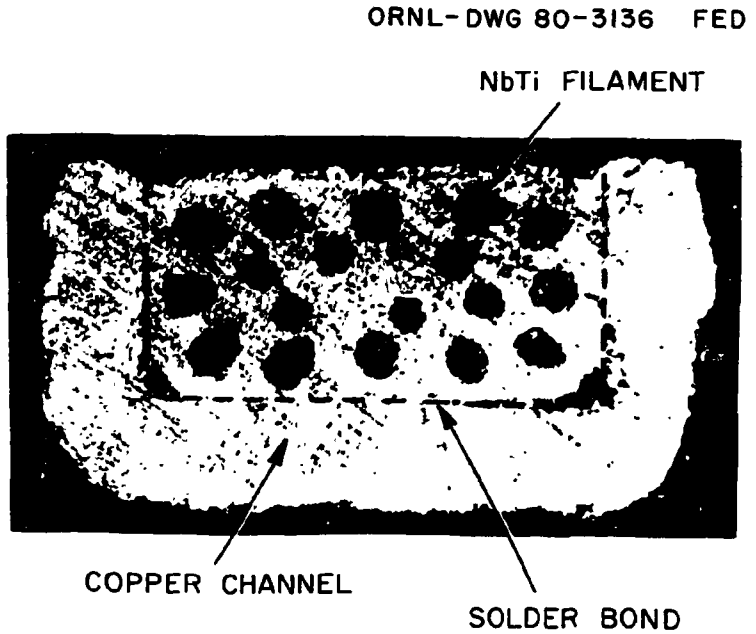

Fig. 4. A photograph of one of the finished conductor cross sections.

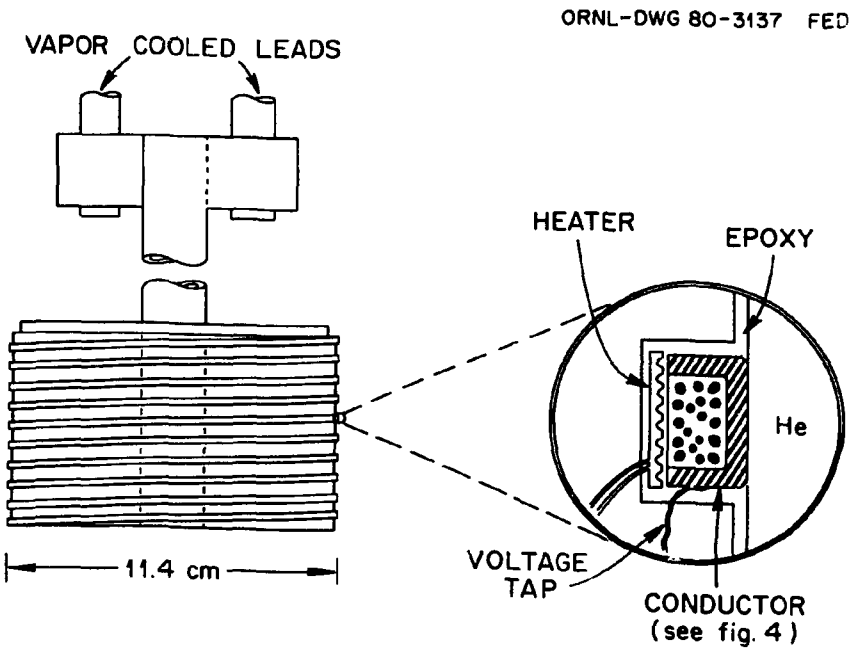

Fig. 5. A sketch of the fiberglass cylinder showing the location of the heater, the conductor, and the epoxy potting.

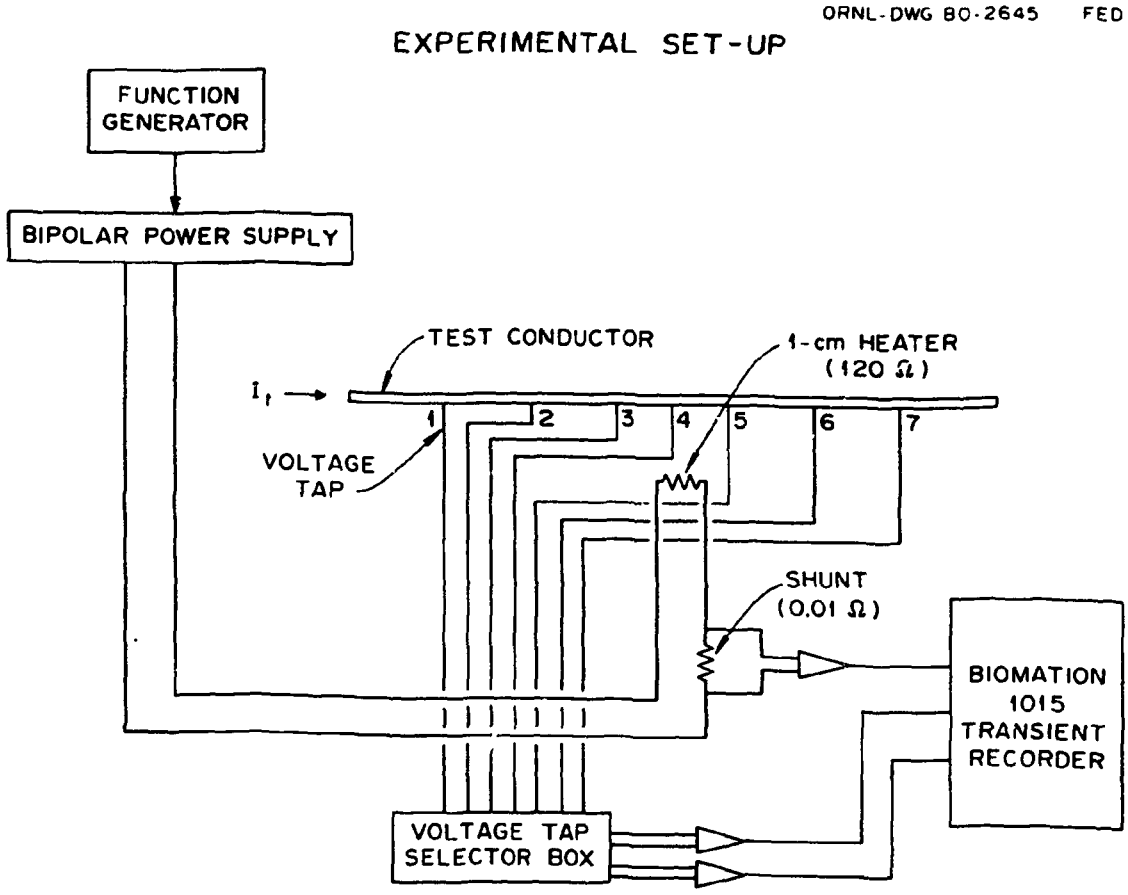

Fig. 6. A schematic drawing of the instrumentation.

7. PROCEDURE

The heater was energized with 2-ms square pulses of increasing power until the conductor just quenched. For slight changes in energy input about this point, temperature profiles of considerably different time durations developed; we assume that a nearly constant voltage drop is indicative of a nearly steady temperature profile. In Fig. 7 the voltage drops are plotted across the longest lasting zones we could make as a function of transport current for three magnetic fields. Appended to representative data points are the time durations over which the voltages were steady. Figures 8a and 8b are oscilloscope traces of representative voltage drops as functions of time: traces 8a and 8b correspond to I = 400 A and I = 575 A, respectively (sample #3, B = 7.5 T). Because of its long duration, trace 8a probably corresponds to a temperature profile approximating the MPZ profile, but trace 8b probably does not.

We also measured propagation velocities for the three conductors at various magnetic fields and transport currents, which are plotted in Fig. 9. Extrapolation of these curves to v = 0 at fixed B gives the minimum propagating currents (I_{MP}).

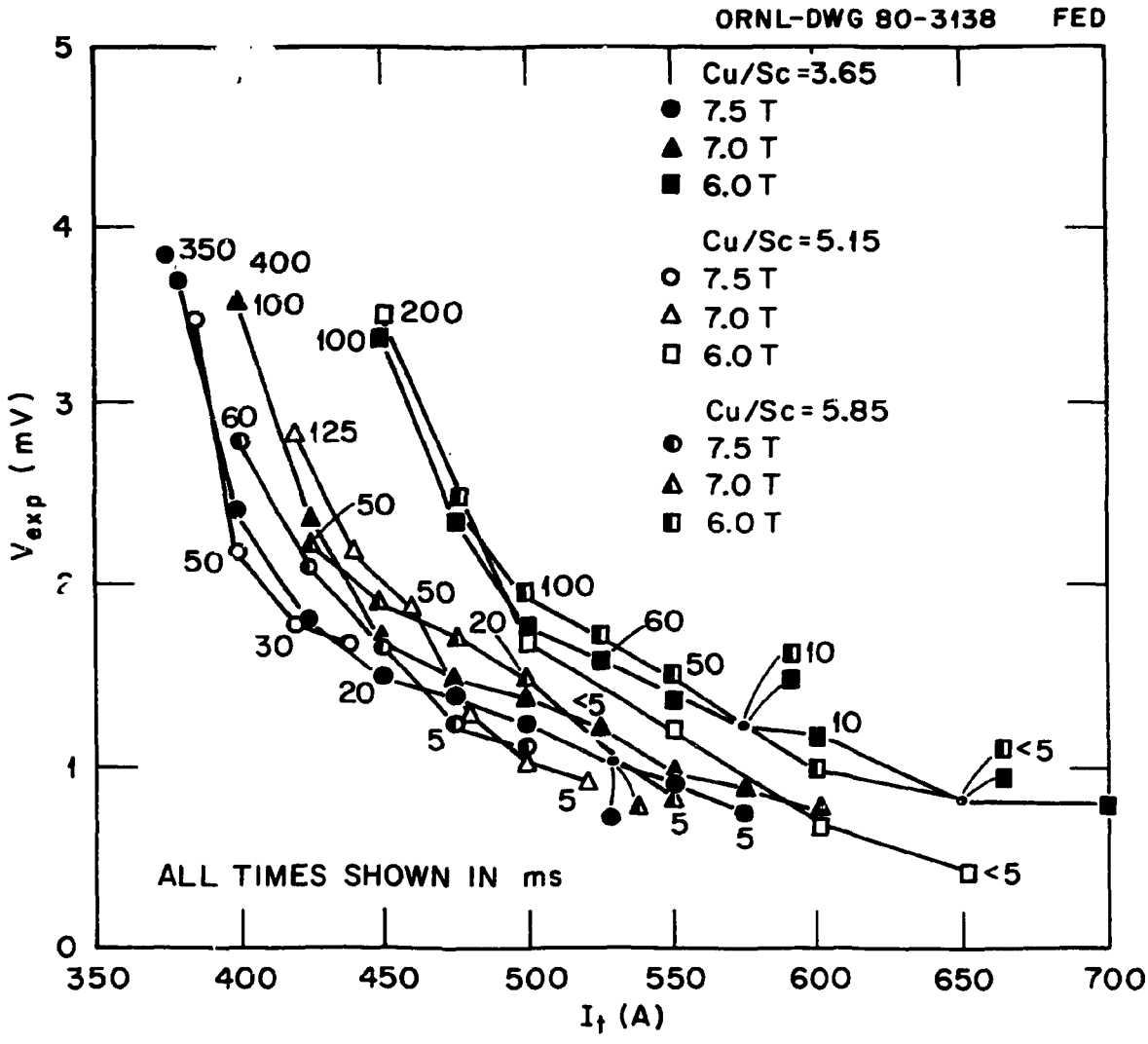

Fig. 7. The voltages across long-lasting normal zones. The numbers attached to the points are the durations, in ms, of the voltages.

ORNL-DWG 80-2649R FED

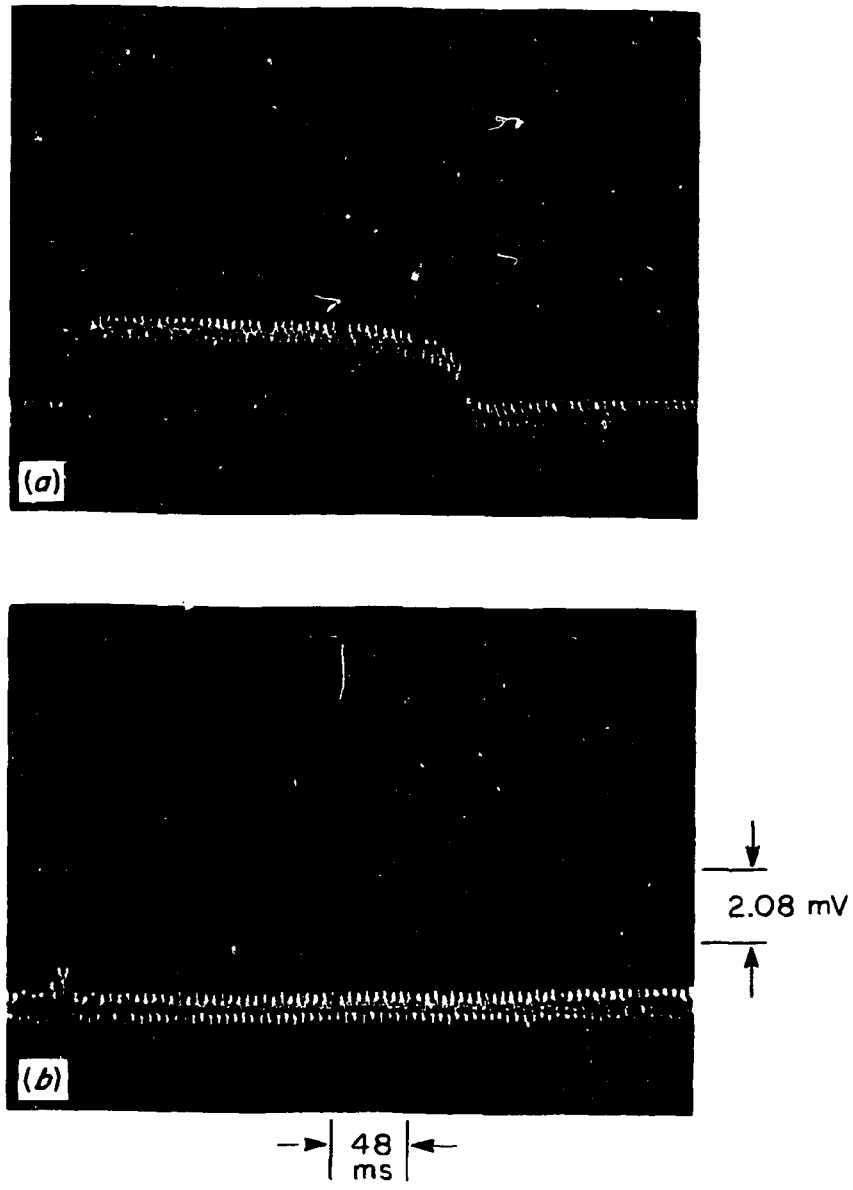

Fig. 8. Typical oscilloscope traces of the voltage across the normal zone as a funciton of time.

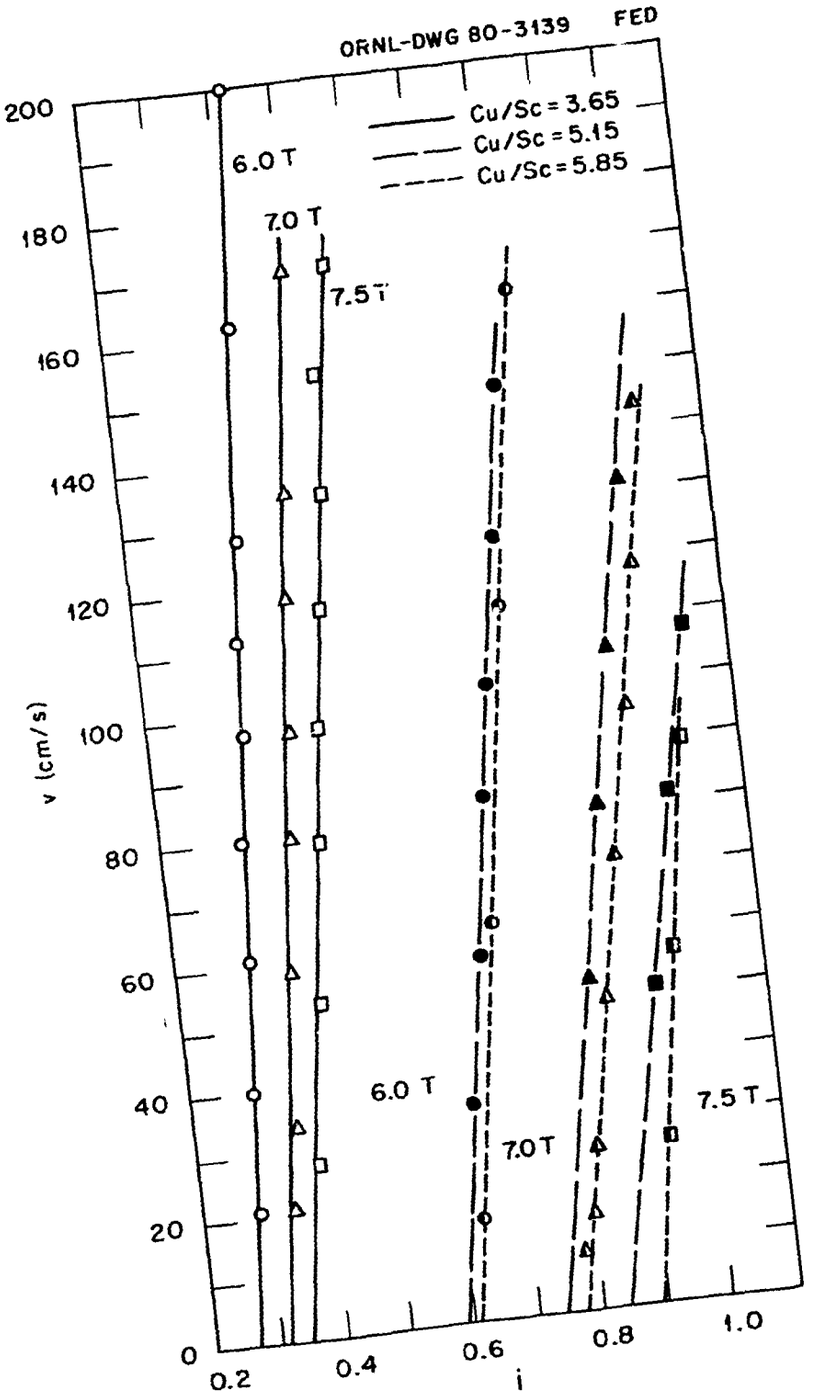

Fig. 9. The propagation velocity for each of the three conductors as a function of field and dimensionless current.

8. DISCUSSION

By assuming a constant heat transfer coefficient, one can apply the equal-area criterion for stability to obtain

$$\alpha = \frac{2 - i_{MP}}{i_{MP}^2} , \tag{16}$$

and, then, obtain h from the definition of α,

$$\alpha = \frac{\rho I_{cr}^2}{fAPh(T_{cr} - T_b)} . \tag{17}$$

T_{cr} is closely given by $T_{cr} = 9.09 - 0.439\ B$ (see Ref. 7) for Nb-46% Ti (B in T, T_{cr} in K). By comparing Eqs. (6b) and (11a), we see that

$$V = 2\left(\frac{kA}{hP}\right)^{1/2} \frac{I\rho}{fA}\,\epsilon . \tag{18}$$

Using Eq. (11b) for the range $\alpha i^3 > 1$ and Eq. (14b) for $\alpha i^3 < 1$, we can calculate V. We use a value of k obtained by applying the Wiedemann-Franz Law[8] at the average of T_{max} and T_b:

$$k = \frac{2.45 \times 10^{-8} V^2 K^{-2}}{\rho}\left(\frac{T_b + T_{max}}{2}\right); \tag{19}$$

T_{max} is calculated using Eq. (9), where

$$\tau_0 = \frac{T_{max} - T_b}{T_{cr} - T_b} . \tag{20}$$

Shown in Fig. 10 is the ratio V_{exp}/V_{calc} for the test conductors as a function of the dimensionless current i. As $i \to 1$, V_{exp}/V_{calc} becomes

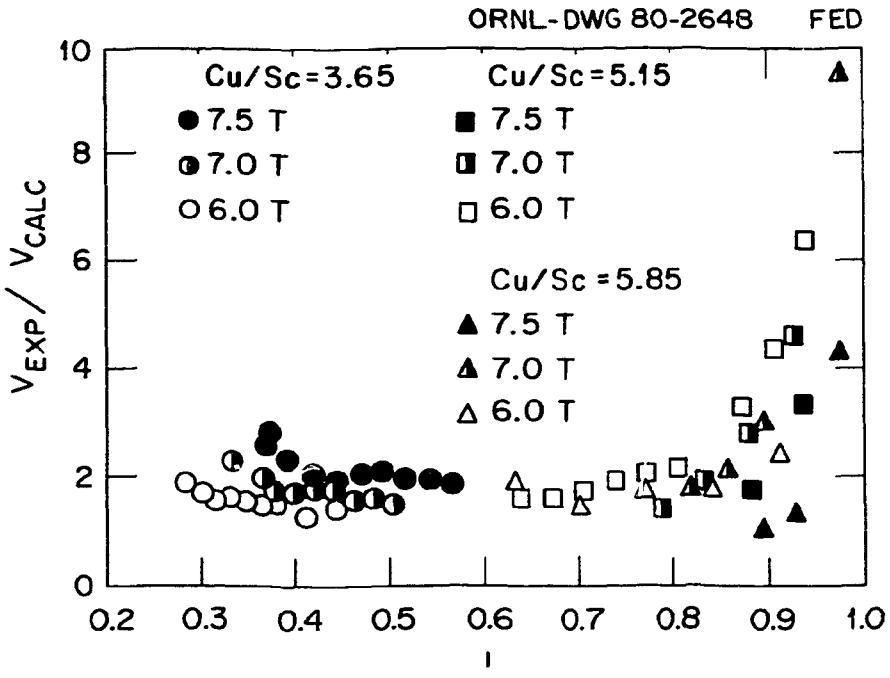

Fig. 10. The ratio of the experimental to the calculated normal zone voltage.

very large, but the experimental values for V at $i \to 1$ probably are not reliable (see discussion of Fig. 8b in Sect. 7). For $i < 0.9$, $V_{exp}/V_{calc} \sim 2$.

The most likely source of error in the theory presented above is the assumption of a constant heat transfer coefficient. Boiling heat transfer coefficients vary greatly with surface conditions and ΔT. A more realistic boiling curve would be a three-part curve like that of Fig. 11a; the corresponding heat transfer coefficient is shown in Fig. 11b. The constant value of h used in our simple model should now be replaced by an effective heat transfer coefficient $\bar{h}$ lying somewhere between the extremes shown in Fig. 11b.

Instead of using the value of h given by Eqs. (16) and (17), we now find the $\bar{h}$ which makes $V_{exp} = V_{calc}$. Plots of $\bar{h}$ vs T_{max} are shown in Fig. 12. In order to further understand the curves of $\bar{h}$, we did three things:

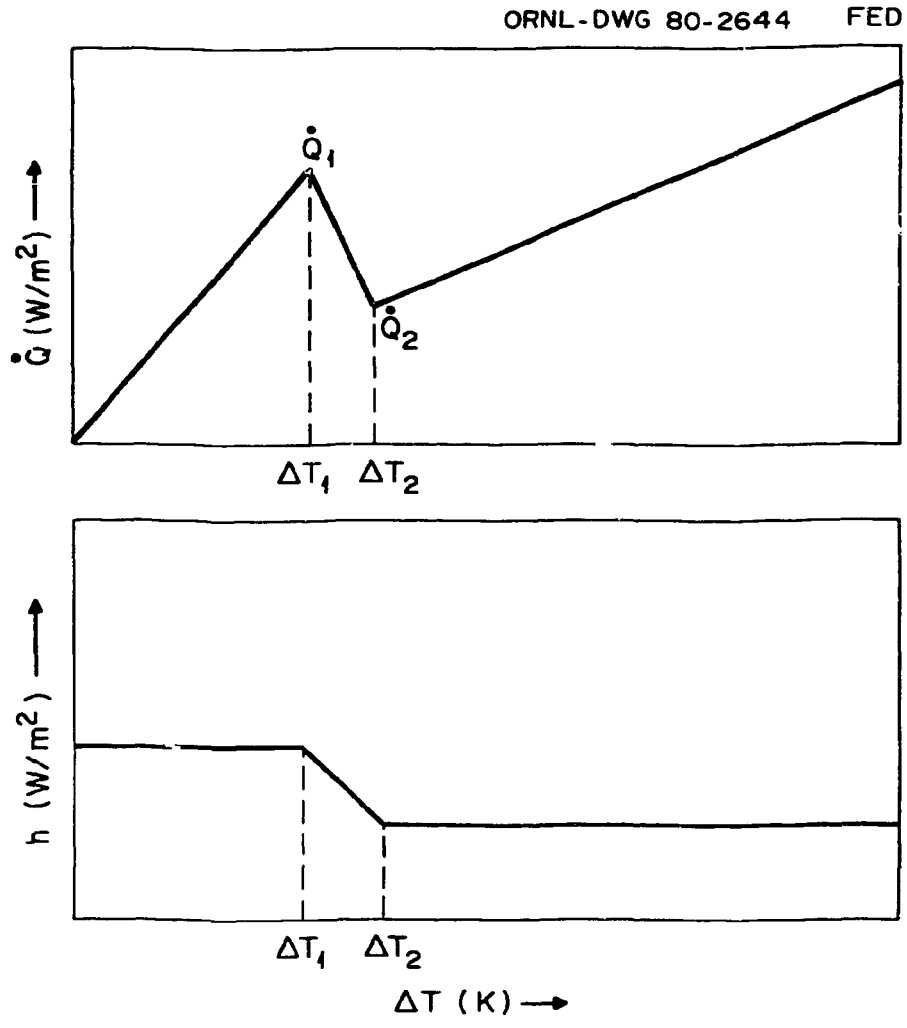

Fig. 11. A sketch of a three-part boiling curve and its associated heat transfer coefficient.

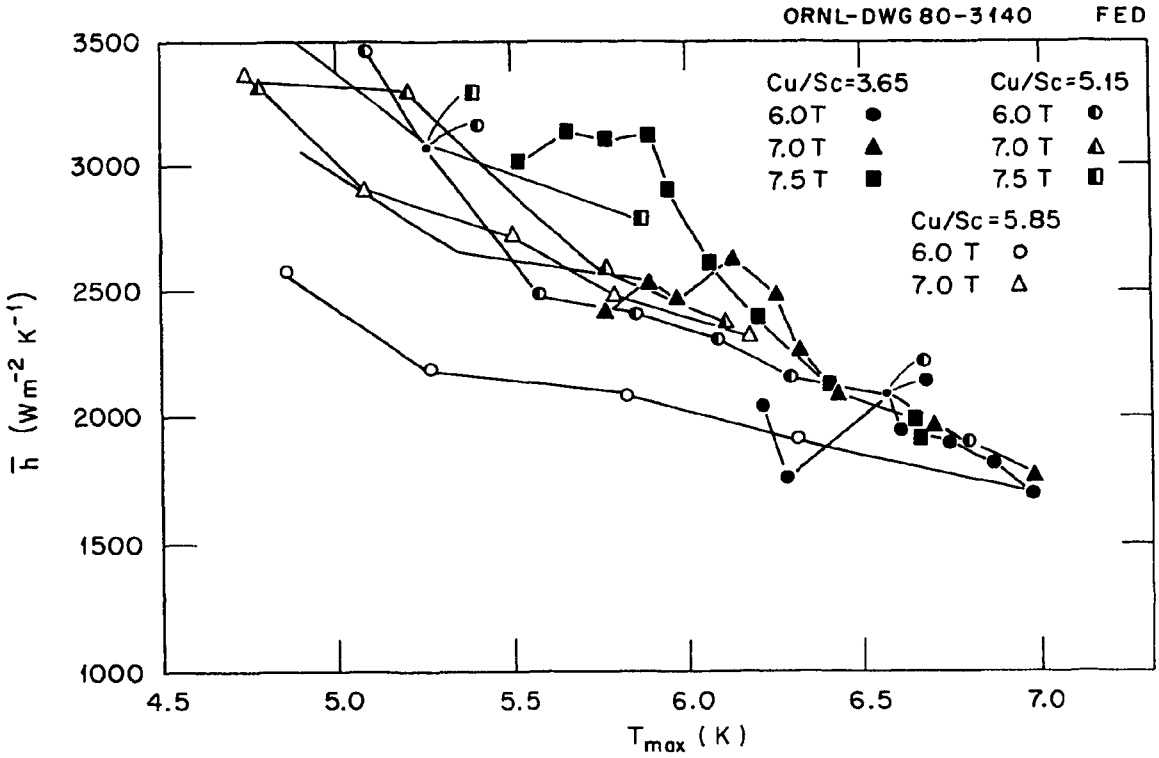

Fig. 12. A plot of the effective heat transfer coefficient $\bar{h}$ versus T_{max}, the maximum normal zone temperature.

(1) We simulated further experiments on a computer by numerically integrating the heat balance equation [Eq. (1)]. The computer program assumes a three-part boiling curve and variable thermal conductivity (given by the Wiedemann-Franz Law evaluated at T) and gives V and E directly.

(2) We used the values of V from step (1) as new data for the simple model, thereby giving $\bar{h}$.

(3) We changed parameters in the three-part boiling curve of step (1) to observe the resultant changes in $\bar{h}$.

Assuming initially that $T_{max} - T_b > \Delta T_2$, as T_{max} decreases, one sees that the weighted average of h increases (see Fig. 11b). Near $T_{max} - T_b = \Delta T_2$ and $T_{max} - T_b = \Delta T_1$, one would expect changes in $d\bar{h}/dT_{max}$, and for $T_{max} - T_b < \Delta T_1$, one would anticipate $\bar{h}$ = constant. The curves

for f = 0.785 seem to be consistent with such an analysis. We nearly duplicated the curve of $\bar{h}$ vs T_{max} for f = 0.785 and B = 7.5 T by assuming:

$\Delta T_1 = 1.6$ K $\quad \dot{Q}_1 = 4800$ Wm^{-2}

$\Delta T_2 = 2.0$ K $\quad \dot{Q}_2 = 1000$ Wm^{-2}

$h_{film} = 560$ Wm^{-2} K^{-1}

Plotted in Fig. 13 are simulated and experimental curves of $\bar{h}$ for f = 0.785 and B = 7.5 T, including the values of ΔT_1 and ΔT_2. The slope of $\bar{h}_{simulated}$ does in fact change at ΔT_1 and ΔT_2, and $\bar{h}$ is fairly constant for $T_{max} - T_b < \Delta T_1$.

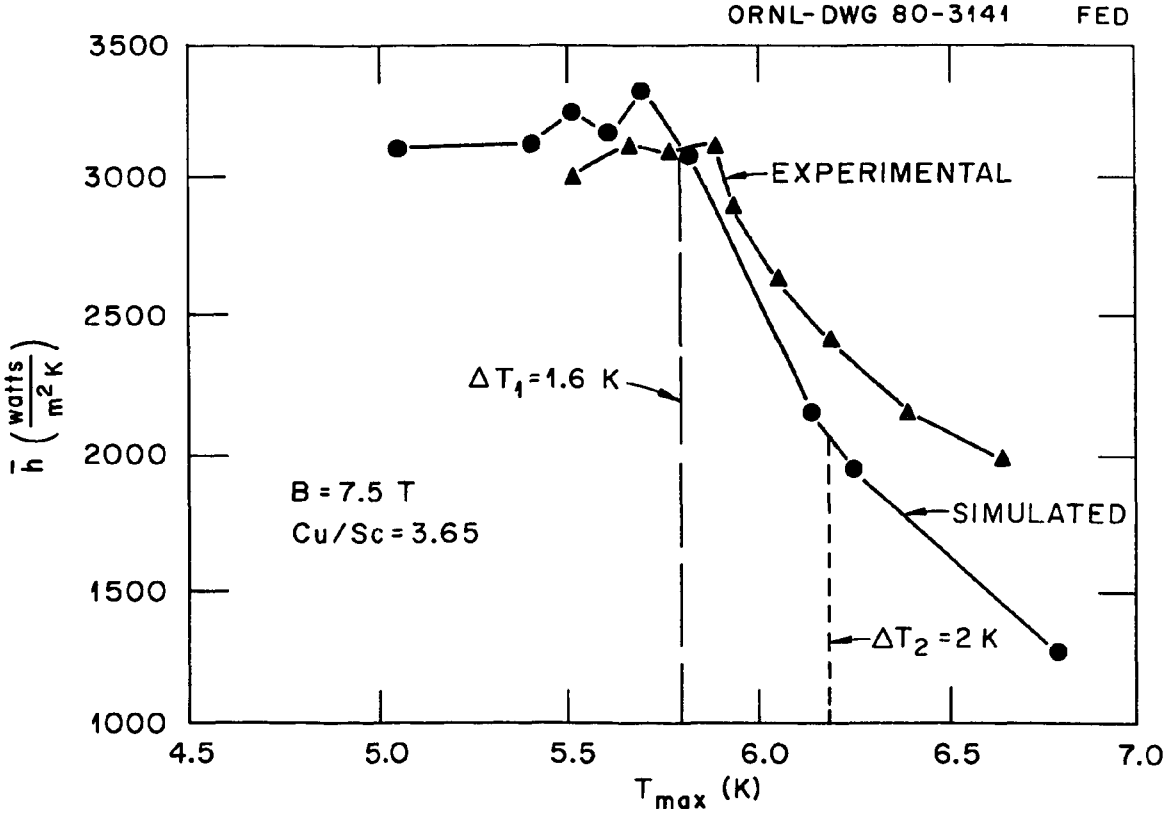

Fig. 13. Simulated and experimental curves of the effective heat transfer coefficient $\bar{h}$ versus T_{max}, the maximum normal zone temperature.

We used the same boiling curve to generate $\bar{h}$ for the 6.0- and 7.0-T data, but unlike the experimental $\bar{h}$, the simulated $\bar{h}(T_{max})$ is the same for 6.0, 7.0, and 7.5 T.

Using $\bar{h}$, we can calculate ε for the data points [see Eqs. (11b) and (14b)]. In Fig. 14, representative values of ε are plotted in the α-i plane, along with theoretical curves of constant ε. Agreement between theory and experiment is good. In Fig. 15, E is plotted as a function of transport current; $\bar{h}$ is used as the heat transfer coefficient; and S is evaluated at $T_{max} + T_b/2$ by using the values of the specific heats of Cu and NbTi given in Ref. 6.

The trend of the MPZ energies shown in Fig. 15 confirms the theoretical expectation that low Cu/SC ratios lead to higher stability than high Cu/SC ratios. A slight complication arises, however, because samples 1, 2, and 3 differ not only in copper fraction but also in the critical current density J_{csc} of the NbTi and in the resistivity ρ of the copper (as noted in Table 2). The uncertainty caused by the differences in J and ρ can be dispelled as follows: at a given field and transport current, the three conductors have the parameters (α_1, i_1), (α_2, i_2), and (α_3, i_3). Can we find a copper fraction f' such that a conductor with J_{csc1} and ρ_1 can have the values $\alpha = \alpha_3$ and $i = i_3$? If we can, then conductor 3 looks like a conductor with the same dimensions and material properties as conductor 1 but with an effective copper fraction equal to f'.

We can in fact do this. If we choose $f' = 0.670$, we can come within a few percent of the values of α_3 and i_3 at all three fields, and if we choose $f' = 0.845$, we can come within a few percent of α_2 and i_2 at all three fields. Thus, using the material properties of sample 1, the three samples have effective copper fractions of 0.854, 0.845, and 0.670. On this basis, we expect E of samples 1 and 2 to be quite close together and that of sample 3 to be substantially larger. This is what is observed, and it confirms our belief that low Cu/Sc ratios are best for stability of metastable conductors.

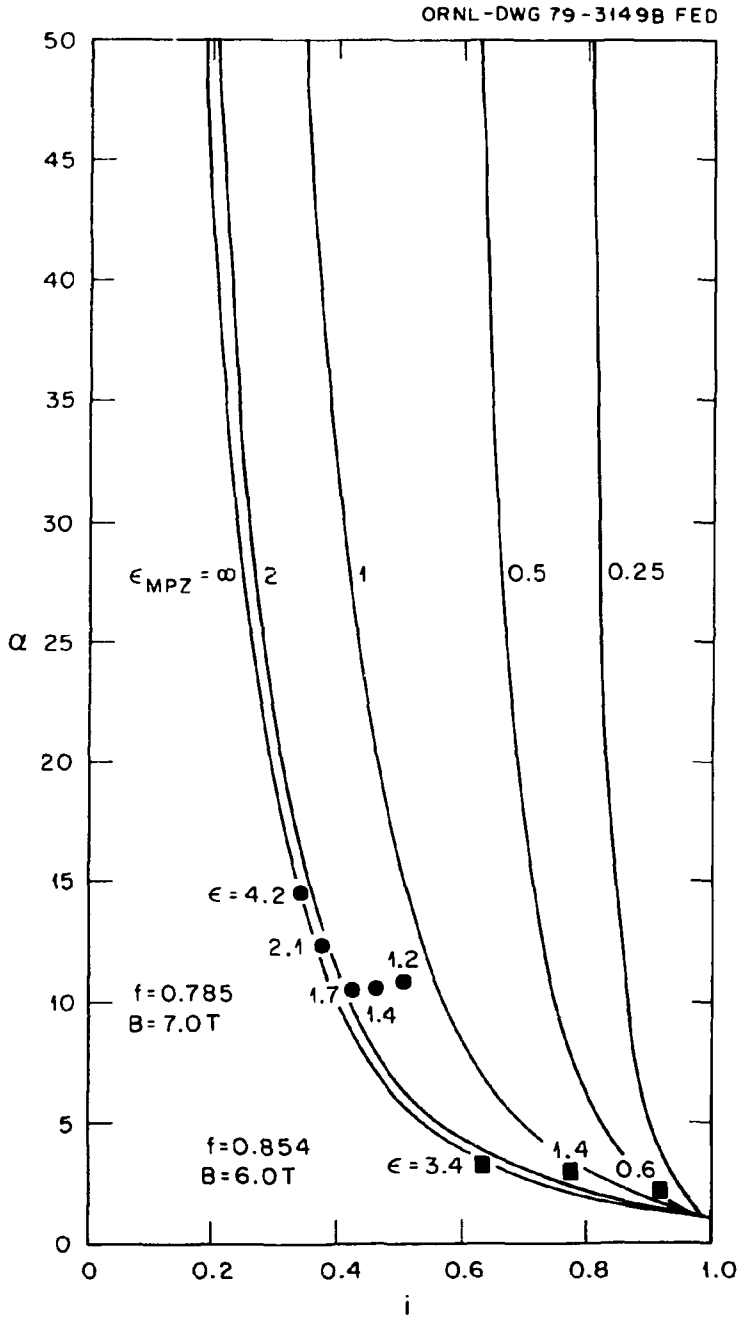

Fig. 14. A plot in the α-i plane of some values of $\underline{\epsilon}$ calculated using the effective heat transfer coefficient $\underline{h}$. The curves are the ε contours from Fig. 2.

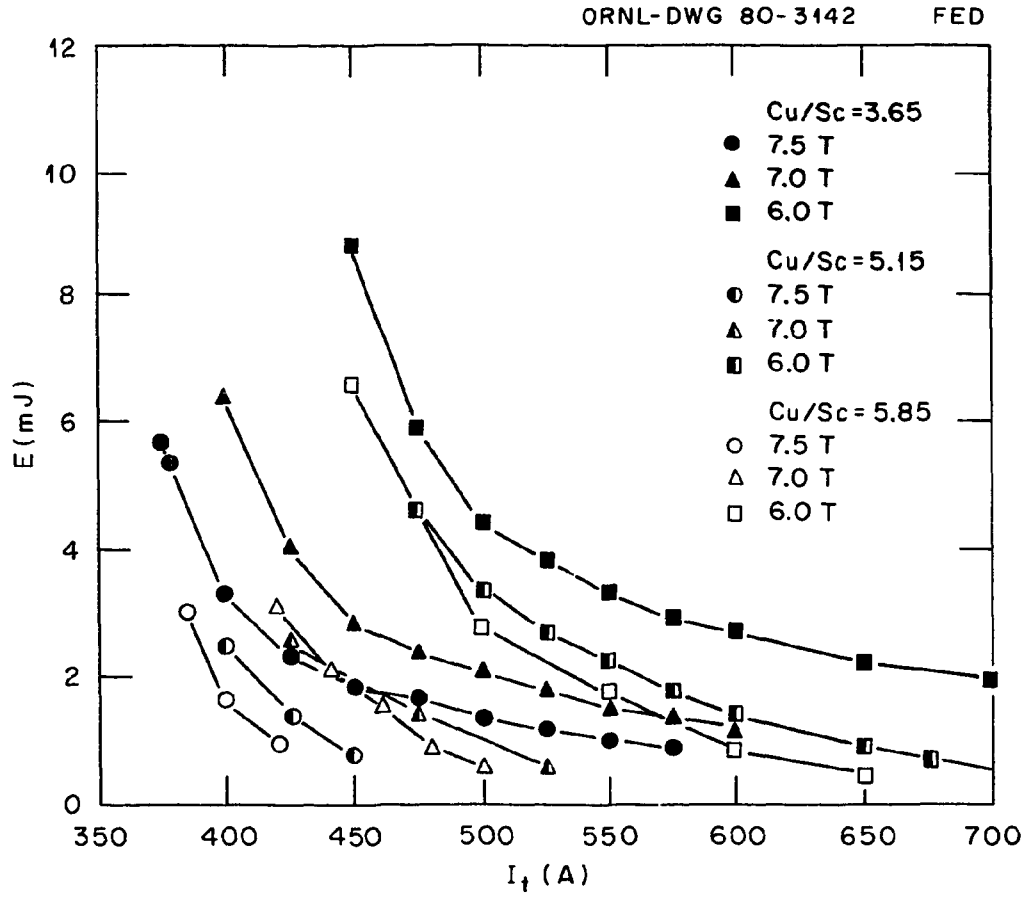

Fig. 15. The energy of the minimum propagating zone as a function of copper fraction, magnetic field, and transport current.

ACKNOWLEDGMENTS

We would like to thank M. S. Lubell for suggesting this problem and to thank J. P. Rudd for his help in preparing the samples.

SYMBOLS

A = cross-sectional area of composite superconductor (m^2)

B = transverse magnetic field (T)

Cu/SC = copper-to-superconductor ratio

E = minimum propagating zone energy (J)

f = volume fraction of copper

h = heat transfer coefficient ($Wm^{-2}K^{-1}$)

$\bar{h}$ = effective heat transfer coefficient ($Wm^{-2}K^{-1}$)

$i = I/I_{cr}$

I = transport current (A)

I_{cr} = critical current (A)

I_{MP} = minimum propagating current (A)

$i_{MP} = I_{MP}/I_{cr}$

J = overall current density (Am^{-2})

J_{csc} = critical current density of superconductor (Am^{-2})

k = thermal conductivity ($Wm^{-1}K^{-1}$)

MPZ = minimum propagating zone

MQE = minimum quench energy (J)

P = cooled perimeter (m)

Q_J = joule heating per unit volume (Wm^{-3})

$s = k(dT/dx)$ (Wm^{-2})

S = volumetric specific heat ($Jm^{-3}K^{-1}$)

Δt = time interval during which heater is energized (ms)

ΔT = temperature difference

T_{cr} = critical temprature (K)

T_b = 4.2 K

V = voltage drop across MPZ (V)

v = normal zone propagation velocity (cm s^{-1})

Δx = heated length of conductor (cm)

$$y = \left(\frac{A}{hkP}\right)^{1/2} \frac{s}{T_{cr} - T_b}$$

$$\alpha = \frac{\rho I_{cr}^2}{fAPh(T_{cr} - T_b)}$$

$$\varepsilon = \frac{E}{2AS(T_{cr} - T_b)(Ak/Ph)^{1/2}}$$

ρ = resistivity of copper (Ωm)

$$\tau = \frac{T - T_b}{T_{cr} - T_b}$$

$$\tau_0 = \frac{T_{max} - T_b}{T_{cr} - T_b}$$

REFERENCES

1. K. Ishibashi, M. Wake, M. Kobayashi, and A. Katase, Cryogenics 19(11), 633-638 (1979).
2. M. N. Wilson and Y. Iwasa, Cryogenics 18(1), 17-25 (1978).
3. B. J. Maddock, G. B. James, and W. T. Norris, Cryogenics 9, 261 (1969).
4. V. E. Keilin, E. Yu Klimenko, M. S. Kremlev, and N. B. Samoilev, in "Les Champs Magnetiques Internes," CNRS, 231 (1967).
5. L. Dresner, IEEE Trans. Magn. 15(1), 328 (1979).
6. Trade-off studies similar to the one being done in this paper have been undertaken by S. Wipf in "Stability and Degradation of Superconducting Current-Carrying Devices," Los Alamos Scientific Laboratory Report LA-7275, Los Alamos, New Mexico (December 1978), p. 50.
7. L. Dresner, J. R. Miller, and G. Donaldson, *Proc. 6th Symp. on Engineering Problems of Fusion Research*, p. 266 (1976).
8. R. G. Scurlock, *Low Temperature Behavior of Solids*, pp. 62-64, Dover, New York, 1966.